MATEC Web of Conferences **33**, 06005 (2015)
DOI: 10.1051/matecconf/20153306005

Structural phase transformations and shape memory effect in ZrCu along with Ni and Hf additions

Tetiana Kosorukova[1,a], Georgiy Firstov[1], Yuri Koval[1], Pavlo Verhovlyuk[1], Jan Van Humbeeck[2] and Henri Noel[3]

[1]*G.V. Kurdyumov Institute for Metal Physics of the National Academy of Sciences of Ukraine, 36 Vernadsky blvd., Kiev 03680, Ukraine*
[2]*MTM Department, Katholieke Universiteit Leuven, Kasteelpark Arenberg 44, B-3001, Leuven (Heverlee), Belgium*
[3]*Institut des Sciences Chimique de Rennes, Université Rennes 1, UMR CNRS 6226, 263 Av. Gal. Leclerc, 35042 Rennes, France*

Abstract. Ni replacement of Cu in ZrCu high temperature shape memory alloy results in the increase of the temperatures of the martensitic transformation (MT) [1]. Once the Ni content reaches 20 at.%, the temperatures of MT are becoming higher than the temperature of crystallization of the amorphous alloy with the same composition [2] and crystallization from the amorphous state in this case takes place through formation of B19` phase without any visible signs of the nanoscale phase separation. In this regard, little is known about the influence of Hf additions onto phase transformations in ZrCu. The present work is dedicated to the study of structure and phase formation upon alloying of ZrCu by Ni and Hf by means of structural and thermal analysis. Their influence onto shape memory behavior will be discussed.

Introduction

It is known that ZrCu-based alloys are considered as perspective high temperature shape memory alloys [3,4]. One of the key issues, regarding high temperature shape recovery in these materials, is proper alloying that must ensure the required temperatures of the MT, strengthening, complicated MT crystallography through the changes in the crystal structure of the austenitic an martensitic phases to avoid plastic deformation in favor of the martensitic one [5].

It was already shown that Ti (replacing Zr) [1] and Co [6-8], Cr [7], Al [8] (replacing Cu) additions lead to the decrease of the MT temperatures, while alloying by Ni resulted in the increase of MT temperatures [1]. It was possible to develop 4 or 5 component ZrCu-based intermetallics with appropriate shape memory characteristics [9,10]. This MT temperatures behavior upon alloying is quite consistent with the views developed in [5,11] that are taking into account electronic and crystal structure changes. According to these views, it was expected that Hf additions replacing Zr should result in the increase of MT temperatures due to the slightly bigger than Zr atomic radius. Anyway, little was known about how Ni and Hf additions influence the crystal structure of ZrCu-based intermetallics. The aim of the present paper was to study structure and phase formation in ZrCu upon Ni and Hf additions with relation to corresponding high temperature shape memory behavior.

Experimental

The alloys for the present investigation were prepared from iodide Zr and Hf and electrolytic Cu and Ni by arc melting under an atmosphere of purified argon. The weight of the ingots was typically 15-25 g. The pellets were turned over and remelted several times in order to ensure good homogeneity. The crystal structure of the samples was analyzed by X-ray powder diffraction (XRD), using a Bruker AXS D8 Advance diffractometer with θ-2θ Bragg-Brentano geometry and monochromatized Cu Kα1 radiation (λ = 1.5406 Å). MAUD software [12] was used for Rietveld refinement. Temperatures and heats of the phase transformations were detected with the help of DSC (Netzsch 404 F1). Shape memory behavior was studied in 3 point bending under the static load in 77-1100 K temperature range.

Results and discussion

Analysis of the X-ray diffraction patterns of the ZrCu-based alloys along ZrCu-$Zr_{50}Cu_{25}Ni_{25}$ and ZrCu-$Zr_{42}Cu_{50}Hf_8$ cross-sections revealed the presence of B19` and Cm martensitic phases like it can be seen for $Zr_{42}Cu_{50}Hf_8$ alloy (Fig. 1). Qualitatively, observed structural states are very much like as it was observed for ZrCu equiatomic intermetallic compound or $Zr_{50}Cu_{25}Ni_{25}$, which crystal and electronic structure was studied and described extensively in [5,13,14]. It was shown in general that MT in these compounds is controlled by the

[a] Corresponding author: tatiana.kosorukova@gmail.com

two types of interatomic interactions (Zr-Cu and Cu-Cu or Ni-Ni). Obviously, Hf additions did not change such situation much. Most of the differences are in the crystal structure parameters of the B19` and Cm phases.

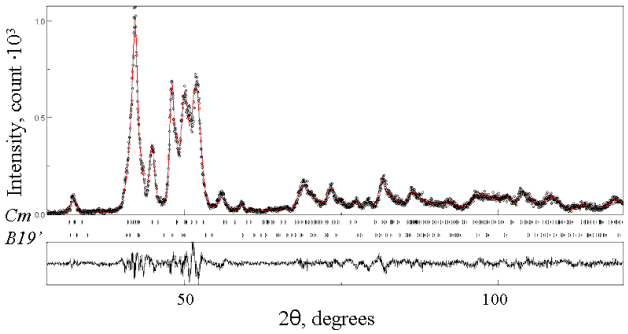

Figure 1. Rietveld refinement results for $Zr_{42}Cu_{50}Hf_8$ - the volume fraction for $P2_1/m$ (B19`) is 20% and for Cm – 80% (R_{wp}=12.6%, R_p=9.2%, R_{exp}=9.0%). Reflections positions for different phases and difference line are also shown.

In the Table 1 the lattice parameters of the observed at room temperatures martensitic phases, their volume fractions and volumes per atom (V/at) are shown for ZrCu, $Zr_{50}Cu_{25}Ni_{25}$ [5] and for $Zr_{42}Cu_{50}Hf_8$ alloys.

Table 1. Crystal structure parameters for phases in ZrCu, $Zr_{50}Cu_{25}Ni_{25}$ [5] and $Zr_{42}Cu_{50}Hf_8$.

Alloy	Phase	a	b	c	β	Volume fraction, %	V/at, Å^3
		Å			°		
ZrCu	B19`	3.299	4.177	5.212	104.2	27	17.406
	Cm	6.356	8.504	5.340	105.5	73	17.383
$Zr_{50}Cu_{25}Ni_{25}$	B19`	3.271	4.118	5.167	103.2	38	16.938
	Cm	6.562	8.279	5.151	103.2	62	17.028
$Zr_{42}Cu_{50}Hf_8$	B19`	3.285	4.042	5.472	104.9	20	17.456
	Cm	6.673	8.266	5.367	106.6	80	17.558

It can be seen generally that Ni additions promote the formation of B19` martensite, while Hf additions lead to the preferential formation of Cm martensite. As for the lattice parameters, it can be also seen that in the case of alloying by Ni only parameter **a** for Cm phase undergone an increase, while all other parameters for both martensites are declining, if compared with binary ZrCu (Table 1). Additions of Hf instead of Zr lead to the increase of the monoclinic angles and parameters **c** for both martensites, as well as **a** lattice parameter for Cm phase, while **b** for both martensites and **a** for B19` undergone a decrease. It can be also seen that addition of 25 at. % of Ni instead of Cu resulted in the volume per atom decrease of about 2% and 2.7%, while addition of 8 at. % of Hf lead to the increase of volume per atom by 0.3% and 1% for B19` and Cm martensites respectively (Table 1). The most affected crystal structure parameters upon alloying by Ni and Hf are volume fractions of both martensitic phases and their volumes per atom. Let us look at these parameters more closely, as they were extracted from the results of the Rietveld refinement of X-ray diffraction patterns obtained from the alloys of ZrCu-$Zr_{50}Cu_{25}Ni_{25}$ and ZrCu-$Zr_{42}Cu_{50}Hf_8$ cross-sections. Effect of the alloying by Hf is shown in Fig. 2, while the result of Ni additions can be seen in Fig. 3.

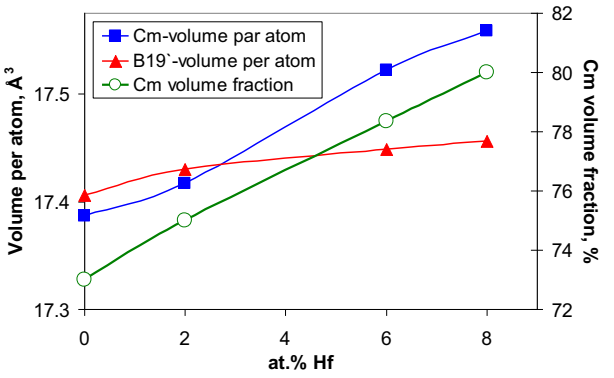

Figure 2. Volume per atom for both martensitic phases and volume fraction of Cm phase changes along ZrCu-$Zr_{42}Cu_{50}Hf_8$ cross-section.

Volume per atom for both martensitic phases is growing in the case of Hf additions but already at 6 at. % of Hf the volume of Cm martensite becomes bigger than B19` contrary to equiatomic ZrCu, where B19` martensite possesses highest volume per atom (Table 1). Volume fraction of Cm martensite increases steadily up to 80% (Fig. 2).

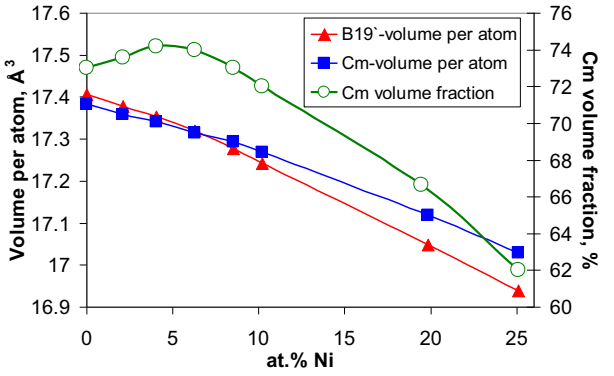

Figure 3. Volume per atom for both martensitic phases and volume fraction of Cm phase changes along ZrCu-$Zr_{50}Cu_{25}Ni_{25}$ cross-section.

In the case of alloying by Ni, shown in Fig. 3, the volume per atom of Cm martensite also becomes bigger than B19` at the increase of Ni content (above 5 at.%) against the background of general decrease of volume per atom for the both martensites. At the Ni content below 5 at.% Cm volume fraction tends to increase but, while its volume per atom becomes bigger than B19`, it starts to decrease at further Ni additions, passing through the maximum around 6 at.%.

It was also important to find out how these structural changes upon alloying by Ni and Hf correspond with thermodynamic characteristics of the MT in ZrCu-based intermetallic compounds. It was shown already [15] that the structural mechanism of MT in equiatomic ZrCu involves specific formation → disappearance of the martensitic crystals of B19` and Cm martensites. It was found with the help of DSC that MT in this compound takes place with wide temperature hysteresis and significant amount of energy dissipates upon complete

MT cycle. Combination of DSC and in situ X-ray diffraction allowed to prove that the origin of wide hysteresis and significant dissipation is related with non-thermoelastic MT in ZrCu, when B19` crystals start to form first during direct B2→(B19`+Cm) MT and disappear first as well on subsequent reverse (B19`+Cm)→B2 MT due to perfect crystallographic match between planes (100) of B2 austenite and B19` martensite [15]. Taking into account two stage DSC behavior and hysteresis loops for B2↔B19` and B2↔Cm transformations extracted from Rietveld analysis of in situ X-ray diffraction patterns with temperature, it was possible to separate heats of the MT for B2↔B19` and B2↔Cm within complete cycle. The same procedure, assuming the same structural MT mechanism, was applied to the DSC results obtained for 2nd complete cycles of MT in $Zr_{50}Cu_{25}Ni_{25}$ and $Zr_{42}Cu_{50}Hf_8$ intermetallics shown in Fig. 4 and Fig. 5 respectively and in Table 2 also.

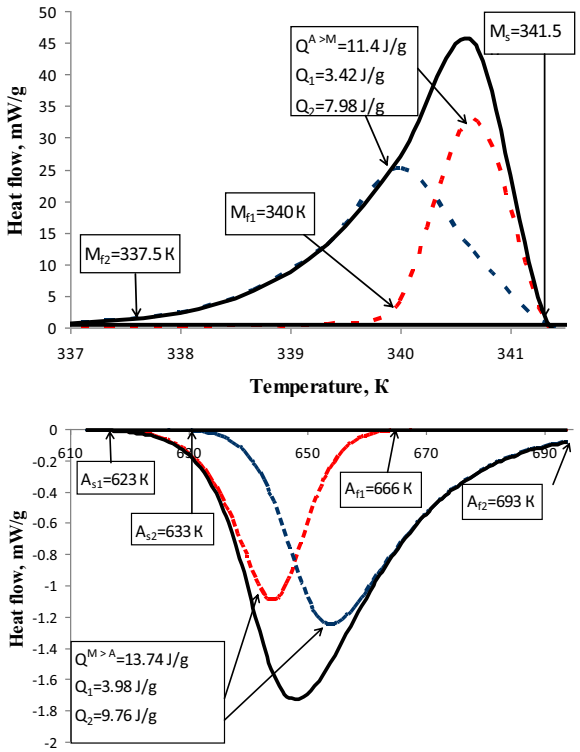

Figure 4. DSC results for complete 2nd cooling-heating MT cycle in $Zr_{42}Cu_{50}Hf_8$ intermetallic treated for two stage behavior with the help of Peakfit 4.06 software package.

It can be seen in Fig. 4 that calorimetric behavior in $Zr_{42}Cu_{50}Hf_8$ intermetallic is very similar indeed to that observed in [15] for binary equiatomic ZrCu compound. Two stage behavior can be clearly seen for the forward (exothermic) and reverse (endothermic) MT. Starting temperature for the forward MT in $Zr_{42}Cu_{50}Hf_8$ intermetallic is the same as for ZrCu but reverse MT starts at As=623 K, which is higher than in ZrCu (As=550 K).

Calorimetric behavior in $Zr_{50}Cu_{25}Ni_{25}$ compound, shown in Fig. 5, confirms the fact that Ni increases MT temperatures in ZrCu. The presence of two calorimetric peaks during forward and reverse MT can be seen also.

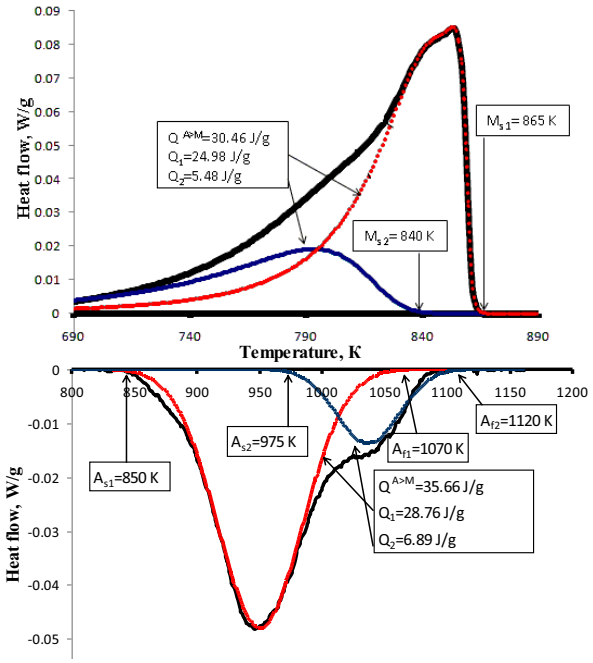

Figure 5. DSC results for complete 2nd cooling-heating MT cycle in $Zr_{50}Cu_{25}Ni_{25}$ intermetallic treated for two stage behavior with the help of Peakfit 4.06 software package.

MT thermodynamic parameters for ZrCu [15], $Zr_{42}Cu_{50}Hf_8$ and $Zr_{50}Cu_{25}Ni_{25}$ compound are summarized in Table 2. Q^F indicates heat released during forward MT on cooling (general B2→M (M=B19`+Cm) or intrinsic B2→B19`, B2→Cm), while Q^R - heat absorbed during reverse MT on heating (general M→B2 or intrinsic B19`→B2, Cm→B2). $Ed=Q^R-Q^F$ and represents energy lost during complete MT cycle according to [16].

Table 2. Ms and As MT temperatures, thermal hysteresis (ΔT), general ($Q^{B2\leftrightarrow M}$, M=(B19`+Cm)) and intrinsic ($Q^{B2\leftrightarrow B19`}$, $Q^{B2\leftrightarrow Cm}$) MT heats and dissipated energy (Ed) in ZrCu [15], $Zr_{50}Cu_{25}Ni_{25}$ and $Zr_{42}Cu_{50}Hf_8$.

Alloy	MT	Ms	As	ΔT	Q^F	Q^R	Ed
		K			J/mol		
ZrCu	B2↔M	340	550	250	977	1345	368
	B2↔B19`		550		343	467	124
	B2↔Cm		578		634	878	244
$Zr_{50}Cu_{25}Ni_{25}$	B2↔M	865	850	210	2320	2714	394
	B2↔B19`				1902	2189	287
	B2↔Cm	840	875		418	525	107
$Zr_{42}Cu_{50}Hf_8$	B2↔M	340	620	318	961	1189	228
	B2↔B19`		620		288	366	78
	B2↔Cm		630		673	823	150

$\Delta T=(A_S+(A_S-A_F)/2)-(M_F+(M_S-M_F)/2)$

It can be seen from Table 2 and Fig. 4 and 5 that MT in ZrCu, $Zr_{50}Cu_{25}Ni_{25}$ and $Zr_{42}Cu_{50}Hf_8$ shows all signs of non-thermoelastic behavior, including wide temperature hysteresis and high levels of the energy lost in a complete MT cycle. Ni additions lead to the significant increase in MT temperatures and to slight reduction of thermal hysteresis, although the dissipated energy is highest in this case. Alloying by Hf results in the widening of thermal hysteresis through the increase of As

temperature, while dissipated energy is smallest amongst considered in Table 2.

Now, let us see how such structure formation during MT upon alloying by Ni and Hf affected high temperature shape memory behavior of ZrCu-based intermetallics. Fig. 6 shows how shape recovery ratio $K_{SME}=(\varepsilon_R/\varepsilon_M)100\%$ (ε_R - recovered strain, ε_M - martensitic strain, accumulated on cooling under the static stress of 300 MPa) depends upon alloying additions.

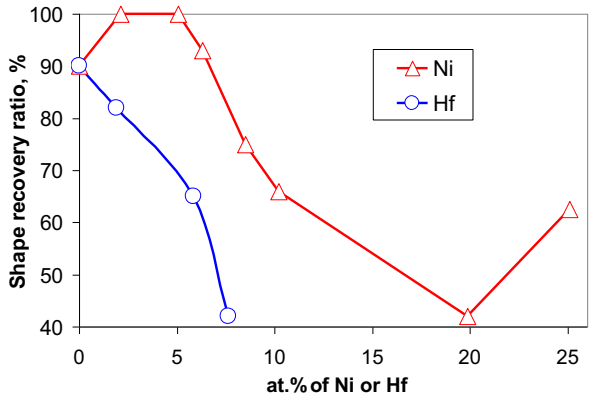

Figure 6. Shape recovery ratio dependence upon Ni and Hf alloying additions.

Alloying by Hf shows decrease in shape recovery ratio, which accelerates above 5 at.%. In the case of Ni alloying additions shape recovery ratio concentration dependence is non-monotonous. Complete shape recovery takes place in the 2-6 at.% Ni concentration range and then drops to a minimum around 20 at.% Ni and rises again to K_{SME}=63% at 25 at.% Ni.

In general, decrease in shape recovery ratio can be attributed to the increase (general or relative) in volume per atom shown in Fig. 2 and 3. As the volume change during forward MT in ZrCu-based intermetallics has a positive sign [5], it is clear that the increase in volume for martensites will result in the rise of internal stresses on the austenite/martensite interface. Stress relaxation by plastic flow ought to be the reason for the incomplete shape recovery.

In the case of Hf additions, acceleration of shape recovery decrease can be linked with the increase of Cm volume fraction that becomes bigger in volume than B19` above 5 at.% (Fig. 2). Plastic relaxation will be more pronounced, which also can be the reason for the widest temperature hysteresis in $Zr_{42}Cu_{50}Hf_8$ (Table 2), where the volume difference of the martensites with austenite must be maximal.

Ni additions lead to the general decrease in volume per atom and growth in Cm volume fraction, which has smaller volume at the initial stage of alloying (up to 6 at.%). Shape recovery ratio grows to 100% (Fig. 6) as most probably the internal stresses are not rising enough for irreversible plastic flow. Maximum in shape recovery (Fig. 6) corresponds to minimal difference in martensites volumes and maximum in Cm volume fraction (Fig. 3). Decrease in shape recovery during further increase in Ni concentration is followed by the decrease in Cm volume fraction, which becomes bigger in volume than B19` at this stage. As for the increase in shape recovery at $Zr_{50}Cu_{25}Ni_{25}$ composition, it might be the result of ordering that has to strengthen the matrix against plastic flow. The indirect sign of such ordering could be the reduction in hysteresis for this composition (Table 2).

It can be summarized that although alloying by Ni and Hf does not change the general character of B2↔B19`+Cm MT in ZrCu, the influence of these alloying additions onto structure parameters and shape memory is not the same. Hf promotes the formation of Cm phase through the increase of volume per atom (weakening of interatomic interaction), which is accompanied by shape memory deterioration. Ni, on a contrary, leads to the decrease in volume per atom (interatomic interaction enhancement), which can be accompanied by improvement in shape memory if minimal volume change during MT is preserved. It can be concluded that the structural changes in ZrCu upon alloying by Ni and Hf has shown the need to control austenite/martensite volume difference through more complicated alloying to ensure complete shape recovery.

References

1. Yu.N. Koval, G.S. Firstov, L. Delaey, J. Van Humbeeck, Scr. Met. et Mat., **31**, 799 (1994).
2. G.S. Firstov, Yu.N. Koval, J. Van Humbeeck, R. Portier, P. Vermaut, P. Ochin, Materials Sci. and Eng. A, **438-440**, 816 (2006).
3. G.S. Firstov, J. Van Humbeeck, Yu.N. Koval, J. Intell. Mat. Sys. and Struct., **17,** 1041, (2006).
4. J. Ma, I. Karaman, R. D. Noebe, Int. Mat. Rev. **55**, 257 (2010).
5. G.S. Firstov, Yu.N. Koval, J. Van Humbeeck, A.N. Timoshevskii, T.A. Kosorukova, P.A. Verhovlyuk, in *Shape Memory Alloys: Properties, Technologies, Opportunities*, ed. N. Resnina, V. Rubanik, 207 (Trans Tech Publications Inc., Zurich, 2015).
6. G.S. Firstov, Yu.N. Koval, J. Van Humbeeck, J. Physique IV, **C5**, 549 (1997).
7. C.A. Biffi, A. Figini Albisetti, A. Tuissi, Mat. Sci. Forum **738**, 167 (2013)
8. W. Gao, X. Meng, W. Cai, L. Zhao, Trans. Nonfer. Met. Soc. of China, **25** (3) 850, (2015)
9. G.S. Firstov, J. Van Humbeeck, Yu.N. Koval, Scripta Materialia, **50**, 243 (2004).
10. G.S. Firstov, J. Van Humbeeck, Yu.N. Koval, Mat. Sci. and Eng., A **378**, 2 (2004).
11. G.S. Firstov, Yu.N. Koval, J. Van Humbeeck, R.G. Vitchev, J. Physique IV, **112**, 1075 (2003).
12. http://www.ing.unitn.it/~maud/.
13. G. Firstov, A. Timoshevski, Yu. Koval, S. Yablonovski, J. Van Humbeeck, Mat. Sci. Forum, **738-739**, 15 (2013).
14. G. Firstov, Yu. Koval, A. Timoshevskii, S. Yablonovski, J. Van Humbeeck, Chem. Met. Alloys, **6**, 205 (2013)
15. G.S. Firstov, J. Van Humbeeck, Yu.N. Koval, J. Physique IV, **11**, Pr8, 481 (2001).
16. A. Planes, J.L. Macqueron, J. Ortin, Phil. Mag. Lett., **57**, 291 (1988).